

Chinese cities' air quality pattern and correlation*

Wenjun Zhang¹, Zhanpeng Guan², Jianyao Li²,

Zhu Su^{3,*}, Weibing Deng^{1,*} and Wei Li^{1,*}

¹ *Key Laboratory of Quark and Lepton Physics (MOE) and Institute of Particle Physics,
Central China Normal University, Wuhan 430079, China*

² *College of Physical Science and Technology, Central China Normal University, Wuhan 430079, China and*

³ *National Engineering Laboratory for Educational Big Data,
Central China Normal University, Wuhan 430079, China[†]*

(Dated: March 4, 2022)

Air quality impacts people's health and daily life, affects the sensitive ecosystems, and even restrains a country's development. By collecting and processing the time series data of Air Quality Index (AQI) of 363 cities of China from Jan. 2015 to Mar. 2019, we dedicated to characterize the universal patterns, the clustering and correlation of air quality of different cities by using the methods of complex network and time series analysis. The main results are as follows: 1) The Air Quality Network of China (AQNC) is constructed by using the Planar Maximally Filtered Graph (PMFG) method. The geographical distances on the correlation of air quality of different cities have been studied, it is found that 100 km is a critical distance for strong correlation. 2) Seven communities of AQNC have been detected, and their patterns have been analyzed by taking into account the Hurst exponent and climate environment, it is shown that the seven communities are reasonable, and they are significantly influenced by the climate factors, such as monsoon, precipitation, geographical regions, etc. 3) The motifs of air quality time series of seven communities have been investigated by the visibility graph, for some communities, the evolutionary patterns of the motifs are a bit stable, and they have the long-term memory effects. While for others, there are no stable patterns.

I. INTRODUCTION

Air pollution has attracted increasing attention in recent years, due to its negative effects on the human health and environmental problems [1–3]. The relevant interesting questions include the spatial-temporal pattern of air quality, the propagation of air pollution, the relations between air quality and earth environment, etc. Previous studies in this domain would be generally divided into two groups: 1) *Time series analysis*: It was often used to describe some basic features of air quality data [4]. For example, Schwartz [5] found that there are strong correlations between air pollution levels and daily mortality in London. Kim [6] proposed a generalized linear model based on the time series data of ozone in Southern California, the model can effectively capture the seasonal non-stationary in ordinary time series. The relation between AQI and social environment was also studied in [7], they analyzed the AQI of 31 provincial cities of China, and found that the value of AQI is positively correlated with the economic level and population level. 2) *Complex networks*: It is an active area of studying the non-trivial topological features, and relations within the multi-agent systems [8–10]. It could be also used to study the features and evolution of the time series data [11–15]. Representative works, such as, Fan [16] studied the PM 2.5 time series data by networks. The phase spaces are denoted as nodes, and edges are assigned to nodes with higher corre-

lation coefficients. They analyzed the relations between the criteria of correlation coefficients and the topological quantities, the similarities of different cities' air quality. Carnevale [17] use neural network to find the source of air pollutants, and found that the source of PM 10 is the easiest and most accurate to be located. Zhang [18] studied the correlation and scaling behaviors of PM 2.5 time series of different cities of China, and found that the probability distribution of the correlations has two peaks, the weighted degree distributions of networks with different kinds of correlations are also discussed.

Time series analysis and complex networks are two useful metrics for carrying out the quantitative analysis of the air quality data. However, most of the previous works did not consider different cities as a whole system (other than the fluctuations, there should be interactions and correlations), and the geographical factors are not taken into account when analyzing the temporal characteristic of air quality. Therefore, we dedicate to study both the air quality patterns and the correlations of different cities with more complete datasets as we can [19], that is, the AQI series data of totally 363 cities from Jan. 2015 to Mar. 2019.

Through calculating the Pearson Correlation Coefficients [20] of AQI series data between each pair of cities, we construct the AQNC by using the PMFG algorithm [21–23]. The probability distribution of the geographical distances of cities which have direct links in AQNC shows that the air pollution has a strong correlation within 100 km and this correlation would become weak as the distance increases. Seven communities are detected in AQNC with the modularity maximization algorithm [24], the detection results are reasonable both for the large

* A footnote to the article title

[†] suz@mail.ccnu.edu.cn;

liw@mail.ccnu.edu.cn

wdeng@mail.ccnu.edu.cn;

modularity and the geographical distribution. The air quality patterns of each community are studied by considering the long-term memory effects and geographical environments. To uncover the characteristics of the motifs of AQI series data, we use the visibility graph to explore the evolutionary patterns of motifs.

The rest of the paper is organized as follows. In Section 2, the AQNC is constructed by PMFG, the basic properties of AQI and the correlations of air quality of different cities also studied. In Section 3, the community structure of AQNC is detected, and the patterns of different communities are analyzed by taking into account the regional average Hurst exponents, average Hurst exponents of each city, etc. Section 4 shows the results of AQI evolutionary pattern using the visibility graph method. Conclusions and discussions are made in Section 5.

II. CONSTRUCTION OF AQNC AND CORRELATION OF AQI OF DIFFERENT CITIES

The AQI of China is introduced in 2012, its comprehensive evaluation is based on the pollution index of SO_2 , NO_2 , CO , $PM_{2.5}$, PM_{10} , and O_3 [25]. We collected and processed the daily AQI time series data of 363 cities of China from Jan. 2015 to Mar. 2019 [19]. The AQI time series data is transformed to AQNC by employing the well-known PMFG method. Based on the correlation of AQI of different cities, the geographical distance on the air pollution diffusion has been investigated.

A. The construction of AQNC and some basic properties of AQI

The Pearson Correlation Coefficient is introduced to calculate the relations of AQI time series data of $N = 363$ cities. The $C_{ij}^{t,\delta}$ between cities i and j during the time period δ (whose center time point is t) is defined as

$$C_{ij}^{t,\delta} = \frac{\langle I_i^t I_j^t \rangle - \langle I_i^t \rangle \langle I_j^t \rangle}{\sqrt{[\langle I_i^{t^2} \rangle - \langle I_i^t \rangle^2][\langle I_j^{t^2} \rangle - \langle I_j^t \rangle^2]}} \quad (1)$$

where the I_i^t is the air quality index of city i at time range $\{t - \delta/2, t + \delta/2\}$. After we calculate the $N \times N$ correlation coefficients $C_{ij}^{t,\delta}$ of each city i and city j , we get the air quality correlation matrix.

The correlation matrix of air quality of N cities is transformed to network by using the PMFG method [23]. All the $C_{ij}^{t,\delta}$ are ranked by their values, edges are added between cities i and j from the largest one, but should keep the network as a planar, and $3(N - 2)$ edges will be added in the network. The main advantage of PMFG is that it could keep the minimum spanning tree, while nodes could be connected with less edges.

The average correlation coefficients $\langle C \rangle$ of each pair of cities are calculated for different correlation length δ

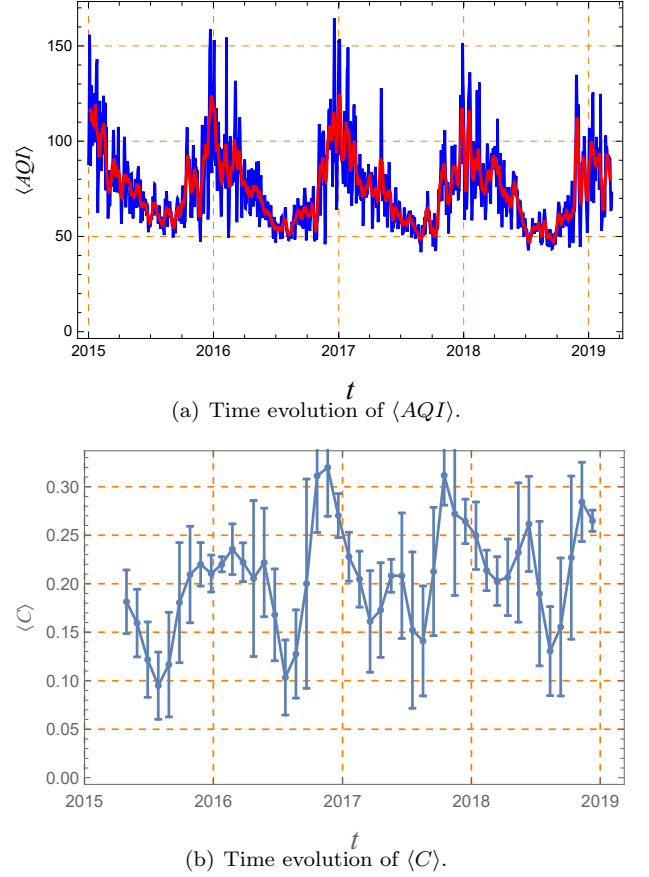


FIG. 1. (Color online) (a) The time evolution of $\langle AQI \rangle$ (average AQI of 363 cities of China). (b) The time evolution of $\langle C \rangle$ (average of correlation coefficients C between all cities with different correlation length δ). The error bars represent the standard deviation of $\langle C \rangle$ for different correlation lengths.

ranging from 30 days to 180 days (in order to reduce the error for only one constant correlation length). The evolutions of $\langle C \rangle$ and the average AQI ($\langle AQI \rangle$) of all cities are shown in Fig. 1. One could find that both $\langle C \rangle$ and $\langle AQI \rangle$ have the one-year cycle. When $\langle AQI \rangle$ is larger, $\langle C \rangle$ also becomes larger. While the peaks of the curve of $\langle C \rangle$ slightly shift to the left compared to that of the curve of $\langle AQI \rangle$. It means that after $\langle C \rangle$ reaches the largest value, the air quality would become worse then.

B. Air pollution diffusion distance

Wind is an important factor that affects the diffusion of air pollutions [18]. Normally the closer the geographical distance of two cities, the stronger the correlation of their AQI would be. Therefore, we investigate the relationship between C of any two cities and their geographical distances, the result is shown in Fig. 2, one could observe that C decreases sharply as the geographical distances increase. When the distance is larger than

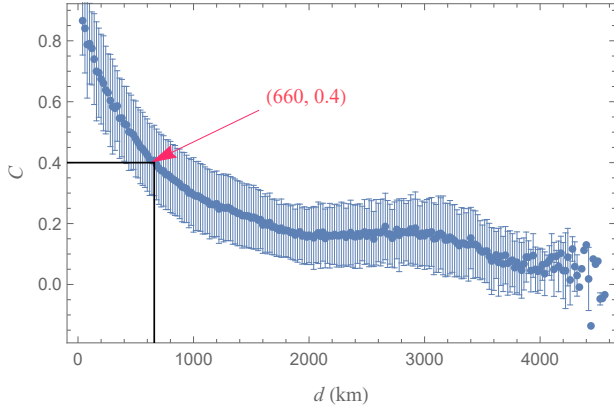
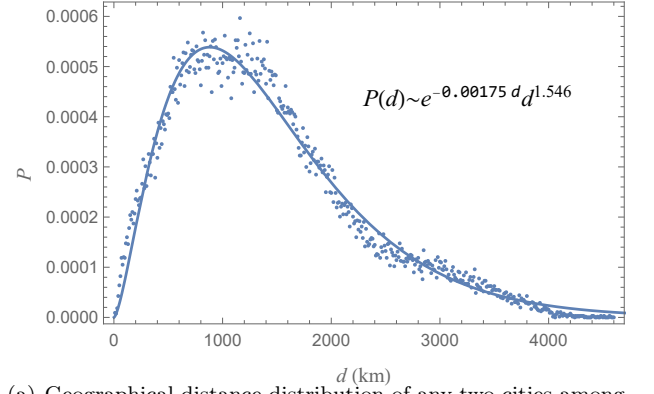


FIG. 2. (Color online) The relationship between the geographical distance d of each pair of cities and their corresponding average correlation coefficients C . Error bars represent the standard deviations of C for each bin of 10 km.

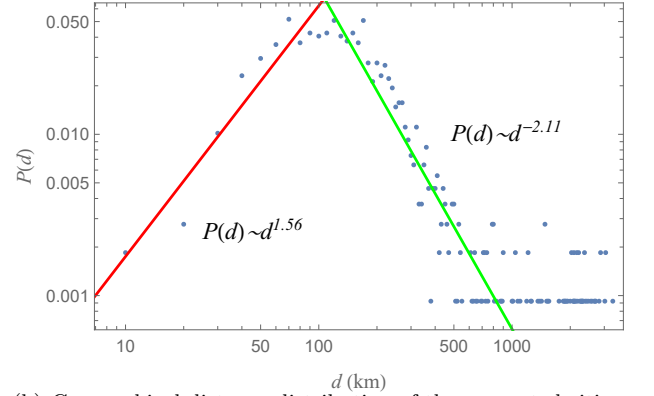
660 km, C becomes smaller than 0.4, which indicates the weak correlation.

Boers [26] studied the global rainfall teleconnections by calculating the probability distribution of distances of links between different places within the network. They found a critical distance of 2500 km, within the critical distance, the rainfall shows a regional weather system, when the distance is larger than 2500 km, the rainfall teleconnections are the global-scale ones. In this realm, we both investigate the probability distribution of geographical distances of any two cities and of the connected cities in the AQNC, the results are shown in Fig. 3. The probability distribution of distances of any two cities follows $P(d) \sim e^{-0.00175d}d^{1.564}$, the peak of the distribution is around 1000 km. But the peak of the probability distribution of distances of links in AQNC is around 100 km. There are two regimes of the distribution, the critical distance is around 100 km. In the region of (10, 100) km, the probability distribution of distance follows $P(d) \sim d^{1.56}$, while in the region of (100, 1000) km, $P(d) \sim d^{-2.11}$. It means that the correlations of AQI series among the cities within 100 km are high, and these amount of cities are connected in AQNC. The correlation will become weak between cities with longer distances.

Furthermore, the relationship between the average AQI (over all the periods) of a single city $\langle AQI_S \rangle$ and its neighboring cities' average AQI $\langle AQI_N \rangle$ have been investigated. Considering the correlation coefficient and geographical distance in Fig. 2, we assign 660 km as the neighboring influential range. Results are shown in Fig. 4(a), one may observe that the higher the average AQI of a city, the higher the average AQI of its neighboring cities. The probability distribution of the correlation coefficients between each city's AQI and its neighboring cities' average AQI is shown in Fig. 4(b), it is obvious that the peak of the distribution is around 0.8, which shows very strong positive correlations. All these results demonstrate that the neighboring cities can have very



(a) Geographical distance distribution of any two cities among 363 cities.



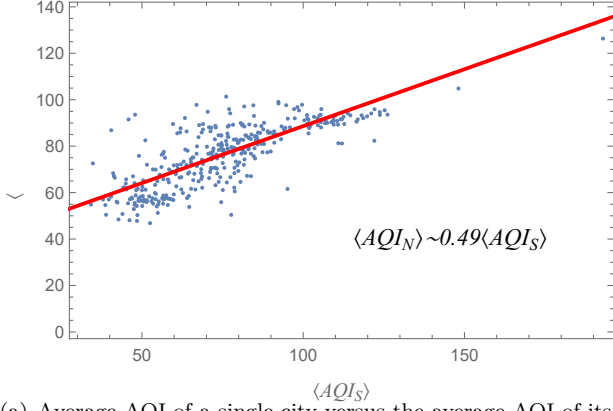
(b) Geographical distance distribution of the connected cities in AQNC.

FIG. 3. (Color online) (a) The geographical distance distribution of any two cities among 363 cities. The peak of the distribution is around 1000 km. (b) The geographical distance distribution of two cities that have direct links in the network. It is plotted in log-log scale, red line is the fitting curve in the range of (10, 100) km, while the green line is the fitting curve in the range of (100, 1000) km.

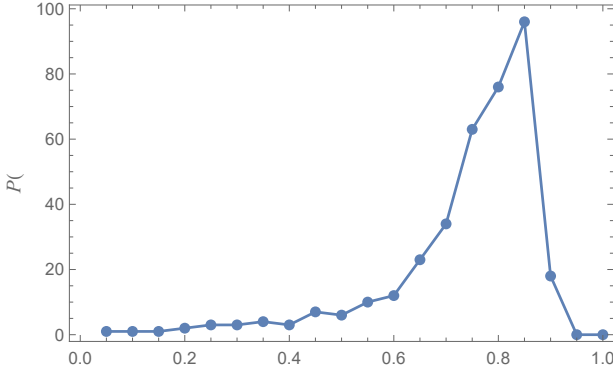
similar AQI patterns.

III. COMMUNITIES OF AQNC AND THEIR PATTERNS

The community structure of AQNC is detected by using Newman's modularity maximization algorithm [27], the result is compared with the geographical location of cities. The Hurst exponents of a city's AQI series data and a community's $\langle AQI \rangle$ series data are calculated, respectively. By taking into account the monsoonal distribution, precipitation distribution and other geographical climate factors, we analyze the different patterns of AQI belonging to different communities.



(a) Average AQI of a single city versus the average AQI of its neighboring cities within 660 km.



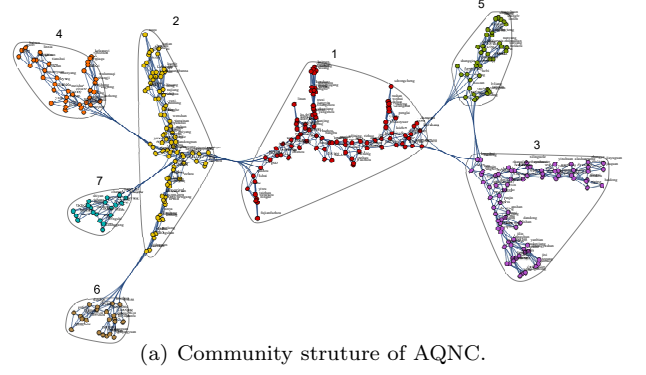
(b) Probability distribution of the correlation coefficients between each city's AQI and its neighboring cities' average AQI.

FIG. 4. (Color online) (a) The relationship between the average AQI of a single city $\langle AQI_S \rangle$ and the average AQI of its neighboring cities $\langle AQI_N \rangle$ within 660 km. (b) The probability distribution of the correlation coefficients between each city's AQI series data and its neighboring cities' average AQI series data.

A. Results of community detection

As shown in Fig. 5(a), seven obvious communities of AQNC have been detected, which modularity is 0.76. From Fig. 5(b), one could find that the cities belonging to the same community almost locate in the same region, this indicates that the air quality of a city is largely influenced by its geographical location, i.e., the similar pattern of air quality is mostly due to the similar geographical environment. Therefore, the names of the seven communities and their geographical features are as follows:

- 1) **East China:** Flat area with medium precipitation, close to the East China Sea.
- 2) **Southwest Highland:** Highland area with medium precipitation, lack of wind.
- 3) **Northeast China:** Plenty of wind [28], no monsoon and lack of precipitation.



(a) Community structure of AQNC.



(b) Geographical locations of cities of different communities.

FIG. 5. (Color online) (a) The community detection result of AQNC. It contains 7 communities and the cities of the same community are denoted by the same color. (b) The geographical locations of cities of different communities on the Chinese map, the colors of cities are the same as shown in the left figure.

- 4) **Basin of China:** Basin area with medium precipitation, lack of wind.
- 5) **Central-north China:** Flat area with medium precipitation, lack of wind.
- 6) **Southeast China:** Area with extreme high precipitation, the cities locate on the monsoonal path.
- 7) **Central-south China:** High precipitation and lack of wind.

B. AQI pattern analysis by Hurst exponent and environmental factors

The Hurst exponent measures the long-term memory of time series [29]. We calculate the Hurst exponent by employing the rescaled range analysis (R/S analysis) [30], for a time series of length n , $X = X_1, X_2, \dots, X_n$, the rescaled range is calculated as follows:

$$m = \frac{1}{n} \sum_{i=1}^n X_i, \quad (2)$$

$$Y_t = X_t - m \quad \text{for } t = 1, 2, \dots, n, \quad (3)$$

$$Z_t = \sum_{i=1}^t Y_i \quad \text{for } t = 1, 2, \dots, n, \quad (4)$$

$$R(n) = \max(Z_t) - \min(Z_t) \quad \text{for } t = 1, 2, \dots, n, \quad (5)$$

$$S(n) = \sqrt{\frac{1}{n} \sum_{i=1}^n (X_i - m)^2} \quad (6)$$

Using the above formulas, we can calculate the rescaled range $R/S(n) = R(n)/S(n)$, average all the partial time series by length n , and obtain $R/S(n) \sim n^H$, where H is the Hurst exponent. Values of Hurst exponents of the AQI time series of all 363 cities were shown in Fig. 7(a), and the value of the Hurst exponent H_A of the average AQI time series of all cities is 0.87. These results show that the AQI time series have the strong long-term memory effects, regardless of the climate patterns or geographical locations of the cities.

We average the AQI time series of cities within the same community, and calculate each community's Hurst exponent denoted as H_C (see Table. I and Fig. 7(b)). The community's Hurst exponent H_C was compared with the average Hurst exponent of all single cities within the community (denoted as $\langle H_S \rangle$) in Fig. 6. The H_C is larger than $\langle H_S \rangle$ for each community, since the time series of average AQI of a community has smaller fluctuations. H_C and $\langle H_S \rangle$ are linearly correlated except community 3 (Purple color point) that exhibits an abnormal feature (see Fig. 6). The Hurst exponents of different communities obey their own rules, since for each community, it has its own geographical aggregation effect, therefore we compare the geographical characteristic of each community, including the precipitation, monsoon, wind and regional geomorphic feature, with its Hurst exponent, see Table. I.

From the community view of AQNC, we would conclude as follows: 1) The values of the $\langle H_S \rangle$ and H_C are relatively large in the basin area, due to the very low wind/air exchanges which implies that the AQI time series of the basin area has strong long-term memory. 2) The monsoon and precipitation are negatively correlated with the Hurst exponents of single cities, as well as communities. Since the monsoon and precipitation could influence very large area, so as to break the air pollution accumulative effect, and lessen the Hurst exponents. 3) The wind (local area) could reduce the value of the Hurst exponent of single cities, but could not reduce the value of communities (H_C). Since it can only influence the AQI change in smaller area (single city), and it is not the same as monsoon which can influence large area (the community area).

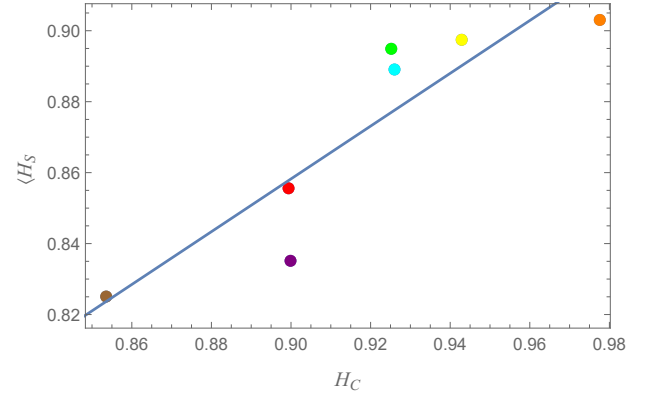


FIG. 6. (Color online) The relation of a community's Hurst exponent H_C versus the average Hurst exponent of all single cities within the community $\langle H_S \rangle$. As can be seen, they are linearly correlated, except community 3 with purple color.

IV. MOTIFS OF AQI TIME SERIES BY THE VISIBILITY GRAPH

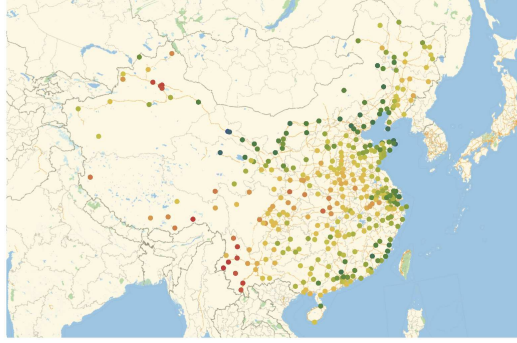
The visibility graph method was used to analyze evolution features, especially the motifs of AQI time series. Some standard motifs were recognized by comparing the original time series with the shuffled ones. We further studied the stability of these motifs of different communities by checking their long-term memory effects.

A. The process and properties of visibility graph

The visibility graph was proposed by Bezsudnov [32] and used to transform the time series to graphs, then these graphs are regarded as vertices to construct a new network [33]. Here, we choose five timing points from t to $t+4$ and set every timing point as one vertex in the network, if two elements (e.g., with height being the value of AQI) at different timing points are visible, they will be connected in the network (see Fig. 8(a)). So we considered each time window with length 5, and set every timing point as a vertex. An edge is added if two vertices (with the height of AQI value) could see each other, for which the direction is from the early timing vertex to the subsequent one. Please find the schematic diagram in Fig. 8. Fig. 8(c) is the corresponding adjacency matrix of the graph in Fig. 8(b). The values of elements on the red line are 1 since they reflect the adjacent timing points. The values of elements below the diagonals are 0. Thus we can represent the visibility graph by the elements above the red line. According to the previous results [34], for 5 timing points, the connection patterns in the visibility graph can be divided into 25 kinds. We denote the network composed of 5 timing vertices as a mode g_t , and the next shifted (only one step) 5 timing vertices as g_{t+1} , and so on. So the time series of AQI can be denoted as $g_t, g_{t+1}, g_{t+2}, \dots, g_{t+n}$. For the next step, we add an edge for any two consecutive mode g_t, g_{t+1} ,

TABLE I. Basic quantities and features of the 7 communities. $\langle AQI \rangle$ is the average AQI of a community through the whole period. H_C is the Hurst exponent of a community. $\langle H_S \rangle$ is the average Hurst exponent of all single cities within the community.

Community label	1	2	3	4	5	6	7
Community color	Red	Yellow	Purple	Orange	Green	Brown	Cyan
$\langle AQI \rangle$	79.42	59.20	76.11	75.48	105.3	51.82	80.73
H_C	0.899	0.942	0.900	0.977	0.925	0.853	0.926
$\langle H_S \rangle$	0.855	0.897	0.835	0.903	0.895	0.825	0.889
Precipitation	Medium	Medium	Low	Medium	Medium	Extreme High	High
Geographical features	Close to ocean, not in monsoon path	Highland	High wind	Basin	Inland	Close to ocean, in monsoon path	Inland



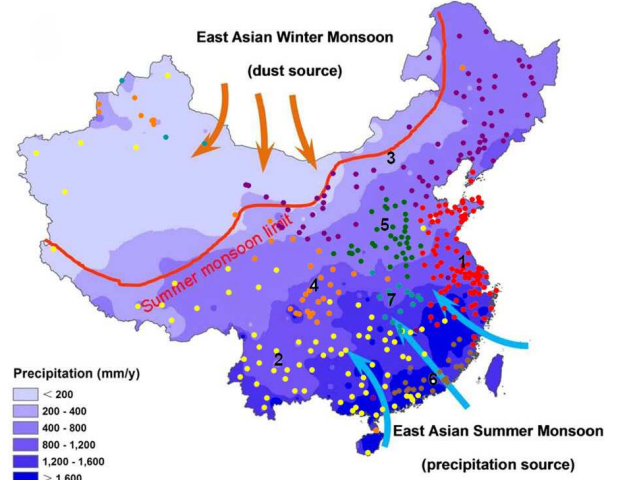
(a) Hurst exponents of 363 cities.



(b) Hurst exponents of 7 communities.



(c) The average AQI of each community.



(d) Community versus geographical environment.

FIG. 7. (Color online) The heat map of the Hurst exponents of (a) 363 cities and (b) 7 communities. (c) The heat map of the average AQI of the 7 communities. (d) The geographical distribution of precipitation and monsoon versus communities (the background map is cited from [31]).

and the same mode of visibility graph as one point, then the network is constituted by 25 visibility graphs, and the mutual transformation can be obtained, which is named as the visibility network. The network is shown in Fig. 9, which could reflect the patterns and rules of AQI evolution. The larger points mean the patterns appear in AQI series much more frequently, and the thicker line means the two patterns have higher probability of transforming from one to another. We calculate the top 8 nodes

with largest frequencies of all communities (shown in Table. II).

B. Characteristics of Motifs of the AQI time series

To investigate the characteristics of motifs of AQI time series, we shuffle the AQI series and construct some new visibility networks, then we compare the frequency of

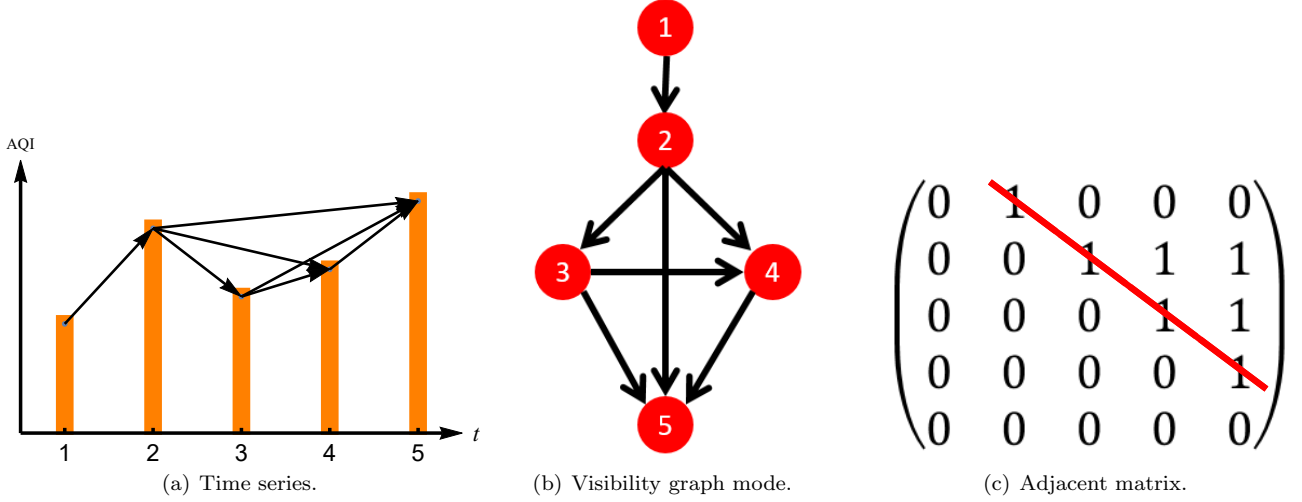


FIG. 8. (Color online) The process of transforming the time series to visibility graph and its corresponding adjacent matrix.

TABLE II. The large frequency visibility graph and corresponding time series of seven communities.

Graph label	256	1	304	19
Visibility graph				
Time series				
Graph label	0	311	257	16
Visibility graph				
Time series				

each visibility graph between the two visibility networks. If the degree of an original visibility network is larger than that of the shuffled visibility network, this visibility graph could be called the “motif pattern”. The different visibility graphs are ranked by the distinction between the original time series and the shuffled one. The top five motifs and corresponding time series of seven communities are shown in Tab. III. The motifs are not the same with the top frequency visibility graphs (Table. II), and the motifs 1 and 2 of all communities are the same.

Then we calculate the Hurst exponents of motifs in seven communities. We implemented the metric [33] of calculating the Hurst exponent of discrete time series with different interval as follows: The top three motifs are chosen to calculate the Hurst exponents of AQI se-

ries. Firstly, we denote the time of the chosen motif as ω_k , where $k = 1, 2, \dots, M$ means the motif is the k -th appeared one in the time series. Then we set

$$\Omega^j = (\omega_{j+1} - \omega_j, \omega_{j+2} - \omega_{j+1}, \dots, \omega_{j+n} - \omega_{j+n-1}), \quad (7)$$

where $j = 1, 2, \dots, M - n$, then

$$\begin{aligned} \Phi^j(i) &= \sum_{w=1}^i [\Omega^j(w) - \langle \Omega^j \rangle] \\ &= \omega_{j+1} - \omega_j - \frac{i}{n}(\omega_{j+n} - \omega_j) \quad (i = 1, 2, \dots, n). \end{aligned} \quad (8)$$

The Hurst exponent can be calculated as

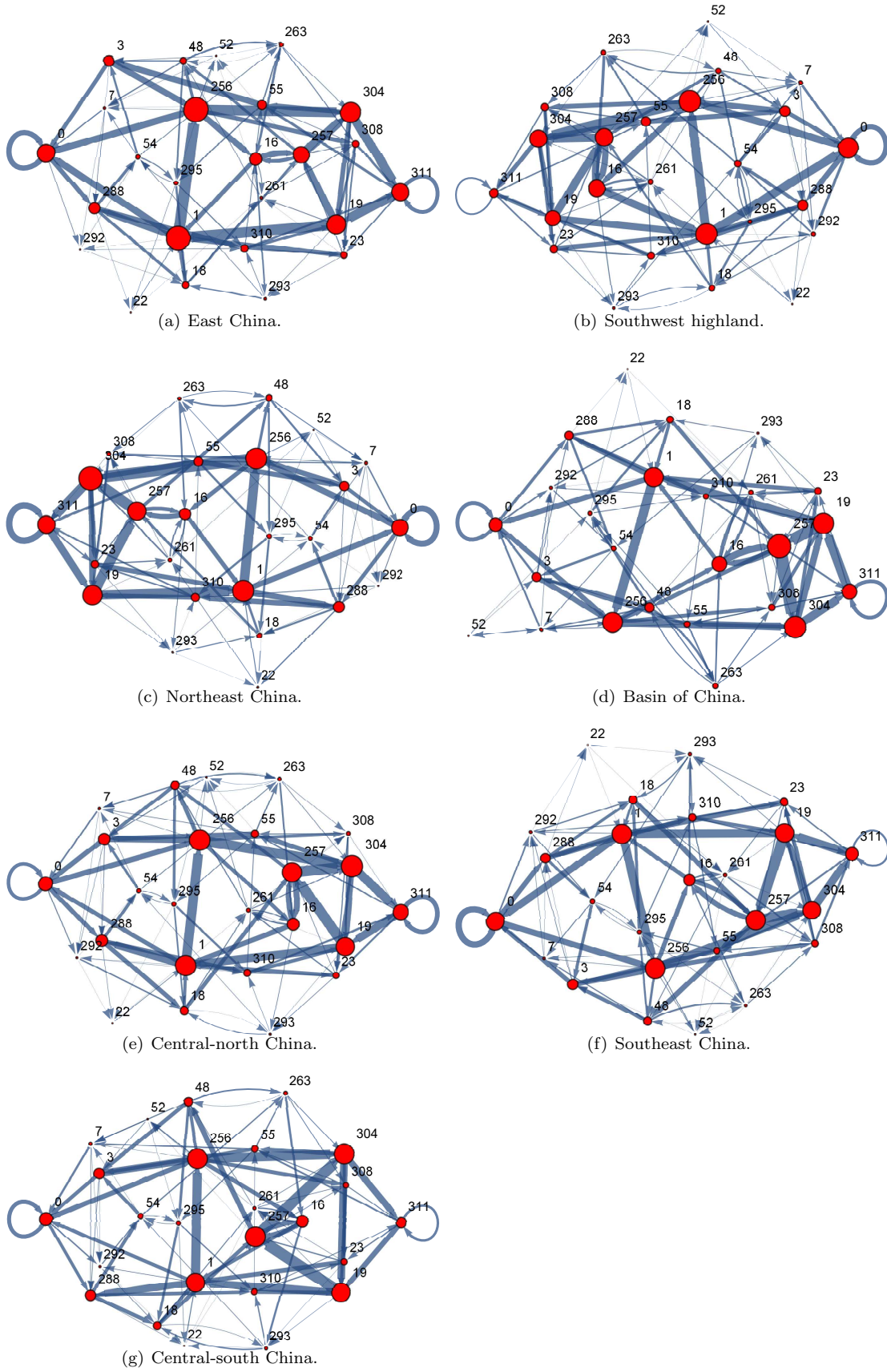
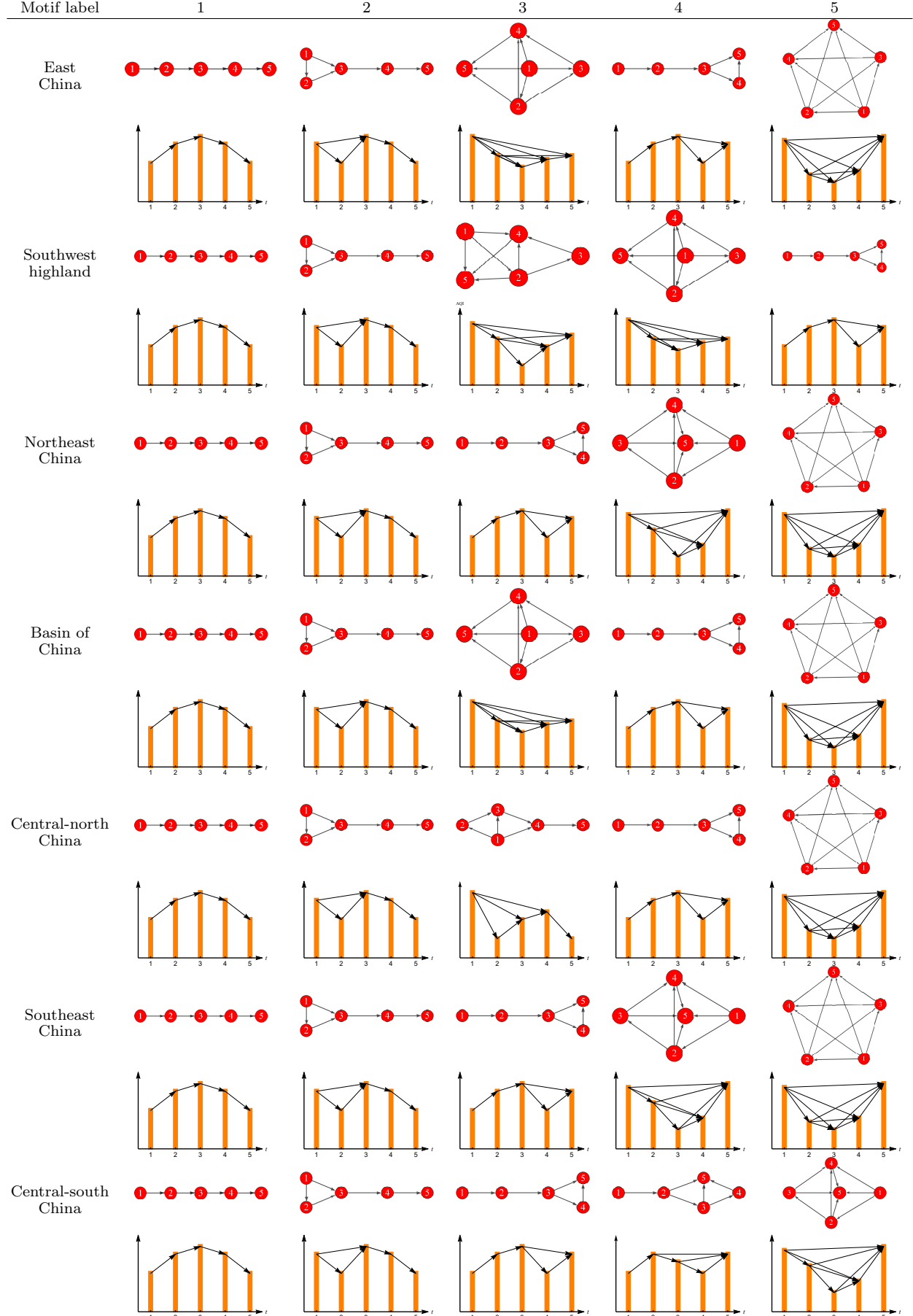


FIG. 9. (Color online) The transforming patterns of the visibility graphs of seven communities, the thickness of the line is proportional to the frequency of that transformation, and the size of the vertex is proportional to the frequency of the visibility graph in the AQI time series.

TABLE III. The top five motifs and corresponding time series of seven communities.



$$R/S(n) = \frac{1}{M-n} \sum_{j=1}^{M-n} \frac{\max[\Phi^j(1), \Phi^j(2), \dots, \Phi^j(n)] - \min[\Phi^j(1), \Phi^j(2), \dots, \Phi^j(n)]}{\text{std}(\Omega^j)}. \quad (9)$$

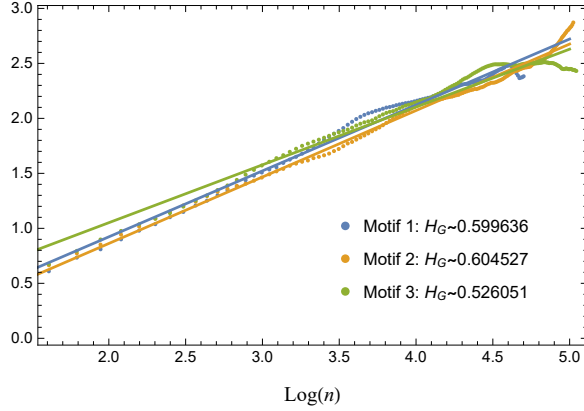


FIG. 10. (Color online) The relation between R/S and n of motifs, it is plotted in log-log scale. The different colors represent different motifs, and the dotted lines are the calculated results, the fitting results are the real lines.

In the relation $R/S(n) \sim n^{H_G}$, H_G is Hurst exponent of the visibility graph pattern. We can calculate H_G by setting n with different values in the range of $(0, M/2)$. Since the fluctuation of AQI series of single city is large, we average the AQI series of all cities within one community, then we can obtain seven AQI averaged series. Since the fourth and the subsequent motifs in each communities have low frequencies, their Hurst exponents could not be calculated, therefore we have only studied the top three motifs, and the relation between R/S and n is presented in Fig. 10 and the H_G exponents of all the communities are listed in Table. IV. Results show that most of the H_G exponents are larger than 0.5 or approximately equal to 0.5. Therefore, the evolutionary patterns have the long-term memory effect and the same motifs always appear in the similar time interval, which means that they are stable.

TABLE IV. The H_G exponent of top three motif in 7 average AQI series, and most H_G exponents are larger than 0.5 or nearly equals to 0.5.

Community label	1	2	3	4	5	6	7
Motif 1	0.599	0.540	0.511	0.481	0.691	0.506	0.683
Motif 2	0.511	0.733	0.598	0.671	0.583	0.445	0.590
Motif 3	0.506	0.424	0.479	0.561	0.532	0.664	0.644

CONCLUSION

We have analyzed the AQI time series from network perspective by using the PMFG method. The correlations of AQI between different cities have been calculated, it is found that there are strong correlations between cities within 100 km. Seven communities of the AQNC have been found, and we observe that the cities in the same community almost distribute in the same region. We have also calculated the regional Hurst exponent and single city's Hurst exponents, respectively, and found that the AQI time series have strong long-term memory effect. Furthermore, we have used the precipitation, monsoon, and geographical environment to explain the pattern of AQI, regional Hurst exponent, and average Hurst exponent of single cities in every community. Lastly, we have transformed the AQI time series to visibility graphs, and got the motifs of seven communities. The Hurst exponents of motifs have been calculated, and results indicate that the evolutionary patterns of AQI in most communities are stable.

ACKNOWLEDGEMENTS

We gratefully acknowledge the fruitful discussions with Rongrong Xie, Longfeng Zhao, and Shengfeng Deng. This work was supported in part by National Natural Science Foundation of China (Grant No. 11505071, 11747135, 11905163, 61873104), the Programme of Introducing Talents of Discipline to Universities under Grant No. B08033 the Fundamental Research Funds for the Central Universities (Grant No. KJ02072016-0170, CCNU, CCNU19QN029, CCNU19ZN012), the China Postdoctoral Science Foundation (Grant Nos. 3020501003).

REFERENCES

- [1] W. Kenneth, C. F. Warner, and W. Davis, Air pollution, its origin and control, Third Edition, Eddison Wesley,

USA, 168 (1998).

- [2] C. A. Pope, M. J. Thun, M. M. Namboodiri, D. W. Dockery, J. S. Evans, F. E. Speizer, and C. W. Heath, Particulate air pollution as a predictor of mortality in a prospective study of u.s. adults, *Am J Respir Crit Care Med* **151**, 669 (1995).
- [3] B. Fakindle, J. Sonibare, O. Okedere, L. Jimoda, C. Ayodele, and C. A. Ng, Air quality index pattern of particulate around a haulage vehicle park, *Cogent Environmental Science* **2** (2016).
- [4] P. J. Brockwell and R. A. Davis, Time series: Theory and methods, *Technometrics* **31**, 121 (1989).
- [5] J. Schwartz and A. Marcus, Mortality and air pollution in london: a time series analysis, *American Journal of Epidemiology* **131**, 185 (1990).
- [6] S. E. Kim, Ordinal time series model for forecasting air quality index for ozone in southern california, *Environmental Modeling & Assessment* **22**, 175 (2017).
- [7] L. J. Xu, J. X. Zhou, Y. Guo, T. M. Wu, T. T. Chen, Q. J. Zhong, D. Yuan, P. Y. Chen, and C. Q. Ou, Spatiotemporal pattern of air quality index and its associated factors in 31 chinese provincial capital cities, *Air Quality Atmosphere & Health* **10**, 1 (2016).
- [8] P. Erds and A. Rnyi, On random graphs i, *Publicationes Mathematicae* **4**, 3286 (1959).
- [9] D. J. Watts and S. H. Strogatz, Collective dynamics of small-worldnetworks, *Nature* **393**, 440 (1998).
- [10] A.-L. Barabási and R. Albert, Emergence of scaling in random networks, *Science* **286**, 509 (1999).
- [11] L. Lacasa, B. Luque, F. Ballesteros, J. Luque, and J. C. Nuno, From time series to complex networks: The visibility graph, *Proceedings of the National Academy of Sciences* **105**, 4972 (2008).
- [12] J. Zhang and M. Small, Complex network from pseudoperiodic time series: Topology versus dynamics, *Physical Review Letters* **96**, 238701 (2006).
- [13] N. Marwan, J. F. Donges, Y. Zou, R. V. Donner, and J. Kurths, Complex network approach for recurrence analysis of time series, *Physics Letters A* **373**, 4246 (2009).
- [14] Y. Yang and H. Yang, Complex network-based time series analysis, *Physica A: Statistical Mechanics and its Applications* **387**, 1381 (2008).
- [15] Z.-K. Gao, M. Small, and J. Kurths, Complex network analysis of time series, *EPL (Europhysics Letters)* **116**, 50001 (2017).
- [16] X. Fan, L. Wang, H. Xu, S. Li, and L. Tian, Characterizing air quality data from complex network perspective, *Environmental Science and Pollution Research* **23**, 3621 (2016).
- [17] C. Carnevale, G. Finzi, E. Pisoni, and M. Volta, Neuro-fuzzy and neural network systems for air quality control, *Atmospheric Environment* **43**, 4811 (2009).
- [18] Y. Zhang, D. Chen, J. Fan, S. Havlin, and X. Chen, Correlation and scaling behaviors of fine particulate matter (pm_{2.5}) concentration in china, *EPL (Europhysics Letters)* **122**, 58003 (2018).
- [19] T. Q. H. Bao, <http://www.tianqihoubao.com/>.
- [20] J. Benestys, J. Chen, Y. Huang, and I. Cohen, Pearson correlation coefficient, in *Noise reduction in speech processing* (Springer, 2009) pp. 1–4.
- [21] L. Zhao, L. Wei, and C. Xu, Structure and dynamics of stock market in times of crisis, *Physics Letters A* **380**, 654 (2016).
- [22] D. Y. Kenett and S. Havlin, Network science: a useful tool in economics and finance, *Mind & Society* **14**, 155 (2015).
- [23] . Tumminello, M., . Aste, T., D. Matteo, T, and R. N. Mantegna, A tool for filtering information in complex systems, *Proceedings of the National Academy of Sciences of the United States of America* **102**, 10421 (2005).
- [24] M. E. J. Newman, Detecting community structure in networks, *European Physical Journal B* **38**, 321 (2004).
- [25] M. China, Ministry of environmental protection of the peoples republic of china, 2015 Report on the State of the Environment in China (2015).
- [26] N. Boers, B. Goswami, A. Rheinwalt, B. Bookhagen, B. Hoskins, and J. Kurths, Complex networks reveal global pattern of extreme-rainfall teleconnections, *Nature* **566**, 373 (2019).
- [27] M. E. Newman, Fast algorithm for detecting community structure in networks, *Physical Review E* **69**, 066133 (2004).
- [28] J. Yang, Q. Liu, X. Li, and X. Cui, Overview of wind power in china: Status and future, *Sustainability* **9**, 1454 (2017).
- [29] H. E. Hurst, Long-term storage capacity of reservoirs, *Trans. Amer. Soc. Civil Eng.* **116**, 770 (1951).
- [30] J. B. Bassingthwaite and G. M. Raymond, Evaluating rescaled range analysis for time series, *Annals of biomedical engineering* **22**, 432 (1994).
- [31] G.-X. Sun, A. A. Meharg, G. Li, Z. Chen, L. Yang, S.-C. Chen, and Y.-G. Zhu, Distribution of soil selenium in china is potentially controlled by deposition and volatilization?, *Scientific Reports* **6**, 20953 (2016).
- [32] I. V. Bezsudnov, S. V. Gavrilov, and A. A. Snarskii, From time series to complex networks: the dynamical visibility graph, *Physica A: Statistical Mechanics & Its Applications* **414** (2012).
- [33] S. Mutua, C. Gu, and H. Yang, Visibility graphlet approach to chaotic time series, *Chaos An Interdisciplinary Journal of Nonlinear Science* **26**, 441 (2016).
- [34] M. Stephen, C. Gu, and H. Yang, Visibility graph based time series analysis, *PloS one* **10**, e0143015 (2015).